Eur Radiol (2008) 18: 993–1004
DOI 10.1007/s00330-007-0848-y

Walter Hundt
Esther L. Yuh
Silke Steinbach
Mark D. Bednarski
Samira Guccione

Comparison of continuous vs. pulsed focused ultrasound in treated muscle tissue as evaluated by magnetic resonance imaging, histological analysis, and microarray analysis

Received: 24 June 2007
Revised: 30 October 2007
Accepted: 21 December 2007
Published online: 19 January 2008

Hundt and Yuh contributed equally to this paper.
Supported in part by the Lucas Foundation and the Phil Allen Truse.

W. Hundt · E. L. Yuh ·
M. D. Bednarski · S. Guccione
Lucas MRS Research Center,
Department of Radiology, Stanford University School of Medicine,
Stanford, CA 94305–5488, USA

W. Hundt (✉)
Department of Radiology, Ludwig Maximilians University of Munich,
Munich, Germany
e-mail: walter.hundt@web.de
Tel.: +49-89-70953620
Fax: +49-89-70958832

S. Steinbach
Department of Otolaryngology Head and Neck Surgery, Technical University of Munich,
Munich, Germany

Abstract The purpose of this study was to investigate the effect of different application modes of high intensity focused ultrasound (HIFU) to muscle tissue. HIFU was applied to muscle tissue of the flank in C3H/Km mice. Two dose regimes were investigated, a continuous HIFU and a short-pulsed HIFU mode. Three hours after HIFU treatment pre- and post-contrast T1-weighted, T2-weighted images and a diffusion-weighted STEAM sequence were obtained. After MR imaging, the animals were euthenized and the treated, and the non-treated tissue was taken out for histology and functional genomic analysis. T2 images showed increased signal intensity and post-contrast T1 showed a decreased contrast uptake in the central parts throughout the tissue of both HIFU modes. A significantly higher diffusion coefficient was found in the muscle tissue treated with continuous wave focused ultrasound. Gene expression analysis revealed profound changes of 54 genes. For most of the analyzed genes higher expression was found after treatment with the short-pulse mode. The highest up-regulated genes encoded for the MHC class III (FC ≈84), HSP 70 (FC ≈75) and FBJ osteosarcoma related oncogene (FC ≈21). Immunohistology and the immunoblot analysis confirmed the presence of HSP70 protein in both applied HIFU modes. The use of HIFU treatment on muscle tissue results in dramatic changes in gene expression; however, the same genes are up-regulated after the application of continuous or pulsed HIFU, indicating that the tissue reaction is independent of the type of tissue damage.

Keywords Focused ultrasound · Muscle tissue · MRI · Histology · Gene expression

Introduction

High-intensity focused ultrasound treatment (HIFU) of a mouse muscle tissue provides a model system to study gene expression patterns at different levels of energy deposition [1]. HIFU causes physical changes in tissues through energy deposition and is undergoing development for diverse therapeutic applications [2]. Tissue being exposed to ultrasound results in structural and/or functional changes. The structural changes range from slight and repairable damage to cell death. The functional changes include tissue proliferation, cell migration, synthesis of various metabolic substances, induction of gene expression, and other important cell changes [3–6].

The different biological effects of ultrasound depending on the tissue type and the physical intensity parameters are known (NCRP 1983). The effects are primary thermal effects, cavitation, and mechanical effects. These three effects function in a different way, because the bioeffects of HIFU depend on intensity and frequency. Thermal effects occur if intensities of several 1,000 W/cm^2 are reached in a focal zone inducing thermal damage of the tissue.

Depending on the temperature, lethal and sublethal effects can be differentiated [7]. Lower frequency favors the occurrence of cavitation. Cavitation can be defined as the interaction between an ultrasonic field in a liquid and a gaseous inclusion (i.e., microbubble) in the insonated medium. This represents a phenomenon unique to biophysical ultrasonics. Lesion formation during HIFU therapy is a complicated process that involves both thermal and cavitation effects [8]. Mechanical effects occur with each ultrasound wave, which has a direct biological effect depending of the tissue type [9]. The mechanical effect is important in the bioeffects of ultrasound. The membrane damage is pivotal in all cellular damage; it is considered to be the most susceptible structure and is exposed to any gross external mechanical stress. The degree of membrane damage and the ability of the cell to repair the damage [10, 11] determines the mode of cell death; it may be instant lysis, necrosis, or apoptosis. In general, energy deposition has been found to modulate various biological processes in tissue cultures and animal models [12]. For example, laser irradiation has been found to increase mitochondrial respiration and ATP synthesis [13] and promote the process of skeletal muscle regeneration after injury [14]. Inflammatory response was markedly decreased by laser irradiation [15], and neoformation of blood vessels in the injured zone of skeletal muscles was elevated [14]. It is known that increased temperature, ischemia, protein degradation, acidosis, oxyradical formation, and increased intracellular Ca^{2+} lead to activation of heat shock protein 72 (HSP 72) [16, 17]. MRI is a very powerful imaging modality and is used in imaging a variety of diseases. One application is the guiding and monitoring of focused ultrasound surgery and other thermal treatments to assess tissue changes taking place during and after therapy [18, 19].

In this study, our aim was to detect and correlate changes in gene expression profiles in muscle tissue treated with various energy levels of HIFU with changes on MR imaging and histology. This can help achieve a better understanding of tissue changes during HIFU therapy with the possibility of finding potential targets for the development of therapeutic or molecular imaging agents.

Materials and methods

All animal experiments were performed in compliance with institutional animal care committee guidelines and with the approval of the animal care committee.

Animal and experimental setup

Fourteen C3H/Km mice aged 10 to 12 weeks were anesthetized with intraperitoneal Nembutal (58 mg/kg) to achieve deep anesthesia. The right and left leg and flank of the body were shaved and all hairs removed using a hair removing cream in order to ensure that hair would not influence the treatment. The mouse body was placed in a plastic tube having a window for positioning and treatment of one muscle side. No movement of the mouse occurred during the FUS treatment. The plastic tube with the mouse body was put into a deionized, degassed water bath to provide a proper ultrasound coupling. The water was heated before the treatment in order to maintain the body temperature. The transducer of the dual ultrasound system (imaging 6 MHz/therapeutic 1 MHz) (Focus Surgery; Indianapolis, IN) was positioned in the water bath. The targeting of the muscle was done by ultrasound imaging of the muscle in the vertical and horizontal plane.

Focused ultrasound system

A modified Sonoblate® system (Focus Surgery; Indianapolis, IN) was used for mechanistic studies. The system contains both imaging and therapy components in a single circular and concave transducer. The therapy portion of the transducer has a frequency (f_0) of 1.0 MHz, an aperture diameter of 50 mm, focal length of 40 mm, a maximum total acoustical power of 120 W, and a maximum focal intensity in water of 8,000 W/cm^2. Focal area was 1.5 mm^2, and the electrical impedance magnitude was f_0 of 81Ω. Efficiency was calculated to be 80%. The imaging portion of the transducer has f_0 of 6.0 MHz, bandwidth of 80%, aperture diameter of 8 mm, and focal length of 40 mm (Fig. 1).

Two different modes of focused ultrasound were applied. Seven animals were assigned to each HIFU mode. In the continuous wave HIFU mode the transducer was powered continuously at 200 mV for 20 s. This sinusoidal wave signal was amplified by a 50-dB radiofrequency power amplifier (Model 2100L, Electronic Navigation Industry, Rochester, NY) coupled to the transducer device (50 Ω impedance).

The dose peak intensity at the focal point was approximately 6,730.6 W/cm^2. For the short-pulsed HIFU mode a cycle of 50 ms with a frequency of 0.5 Hz was applied. The same power was chosen, and the HIFU application lasted for 16.5 min. The resulting average intensity at the focal point was 134.6 W/cm^2. These parameters were led in a calculated total acoustical power of 100.29 W and a pressure of 142.09 kPa. The total energy deposition was nearly the same in both modes (continuous wave HIFU mode 134,613.6 J and short-pulsed wave HIFU mode 133,267.4 J) (Table 1).

MR imaging

A clinical 1.5-T GE Signa MR Scanner (GE Medical Systems, Milwaukee, WI) was used with a wrist coil for signal reception. The animal was imaged 3 h after the application of focused ultrasound. The mouse was placed

Fig. 1 Modified Sonablate™ 200 with ultrasound probe. Experimental setup of the single components ultrasound transducer, high frequency amplifier, diagnostic and therapeutic ultrasound probe and experimental water bath

prone and fixed in wrapped tissue. The body temperature was maintained throughout the MRI studies with a warm blanket. The following scan protocol was carried out in the axial plane with a FOV of 6, 256×192 pixels, slice thickness of 2.0 mm, and two acquisitions: (1) pre-contrast T1-weighted SE (TR/TE 400/15 ms), (2) pre-contrast T2-weighted FSE (TR/TE 4,000/85 ms), ET 12), (3) diffusion-weighted STEAM-sequence (TR/TE/TM 6,000/30/157 ms, voxel size 1.73 cm^3 (1.2*1.2*1.2 cm) located in the muscle tissue of the flank, NEX=3, b-values: 50–250–500–750–1,000–2,000–3,000–4,000 s/mm^{-2}, small Δ: 9 ms, diffusion gradients were applied simultaneously in all three directions in order to achieve higher b-values; T2-time determination (TR/TE 6000/30–50–80–120 ms); (4) post-contrast T1-weighted SE (TR/TE 400/15 ms) at 2 min after the injection of Gd (DTPA) (Magnevist®, Berlex, Wayne, NJ); 200 μl of 0.5 M solution (1:8 dilution) administered via tail vein with a rate of 40 μl/s.

After MR imaging, about 4 h after the application of focused ultrasound, the animals were euthanized and the muscle tissue taken out and snap frozen for histological and microarray analysis.

Image analysis

Post-processing of the MRI images was performed using MRVISION (MRVision Co., Menlo Park, CA) version 1.5.4b for analyzing the tissue pixel intensities of the treated and untreated muscle tissue. For semi-quantitative analysis the mean signal intensities of the muscle tissue and fat tissue were measured on the T2-weighted FSE sequence and the T1-weighted SE sequence before and after contrast medium administration. They were measured using a monitor-defined region of interest (ROI) with ≈250 pixels, including the whole visible MRI changes due to the application of focused ultrasound, and 3–11 pixels for the fat tissue. For measurement at different times, the size and location of the ROIs were kept constant. The signal-to-noise ratios (SNR) were calculated using the mean signal intensities of the areas and the SD of the background noise. The diffusion coefficient and the T2-time of the muscle tissue before and after application of focused ultrasound were determined by using Matlab software version 2.0. The volume of tissue change was determined by using the 3D-method on the T1-weighted SE sequence after contrast medium administration. The area measurements were done manually by tracing the contour of each tomogram of the devascularized non-contrast enhancing area and the contrast enhancing muscle tissue. The volume was calculated as a sum of the area times section thickness. Volumetric analysis was performed off-line at a workstation using analysis software (OSIRIS^R, Digital Imaging Unit, University Hospital of Geneva, Geneva, Switzerland).

Histology and immunohistochemistry

In order to assess the pathological changes due to focused ultrasound, hematoxylin and eosin (H&E) and immunohistochemistry were performed. For the H&E staining the tissue samples were preserved in 10% formalin solution for 96 h. Afterwards they were embedded in paraffin, sectioned, stained with hematoxylin and eosin, and then mounted on the glass slides. Morphologic features used to identify viable nuclei included the absence of overall shrinkage and homogenous dark basophilia.

Table 1 Applied high intensity focused ultrasound parameter

	cw-mode	pw-mode
mV	200	200
Duration	20 s	990 s
Pulse duration		50 ms
Pulse frequence		0.5 Hz
Intensity (W/cm^2)	6,730.7	134.6
Total energy (J)	134,613.6	133,267.4
Pressure (kPa)	142.1	142.1
Total acoustical power (W)	100.3	100.3

For immunohistochemistry, the air-dried slides were fixated in cold acetone for 5 min and dried afterwards for 1 h. The samples were put into a 0.3% hydrogen peroxide solution for 10 min. The sections were incubated with the HSP 70 primary antibody (Stressgen Biotechnologies Inc, San Diego, CA) with a dilution factor of 1:300 for 1 h at room temperature. In a second step the sections were incubated with a biotinylated goat anti-mouse immunoglobulin at a dilution factor of 1:500 (Jackson Immunoresearch Labs) for 30 min at room temperature and incubated with streptavidin-HRP, (Jackson Immunoresearch Labs) for a further 30 min at room temperature. Between the different steps the sections were rinsed in PBS. In the final steps, the sections were reacted with DAB chromogen rinsed in water and counterstained in hematoxylin, dehydrated, cleared and mounted. The slides were reviewed by a veterinary pathologist.

Microarray analysis

The whole treated and the contra-lateral untreated muscle tissue (control) was removed surgically. The tissue samples (>500 mg) were deep frozen at a temperature of –80°C. The total RNA was isolated using TRIzol Reagent® (GibcoBRL Life Technologies, Rockville, MD) and the double stranded cDNA created by using the SuperScript Choice system (Life Technologies). In further steps the cDNA was extracted and precipitated. Biotinilated cRNA was synthesized using Enzo Bio Array High Yield RNA Transcript Labeling Kit (Enzo Diagnostics Inc., Farmingdale, NY). After incubation the labeled cRNA was cleaned according to the RNeasy Mini kit protocol (Qiagen). The cRNA was fragmented and hybridized on the murine Genome U74Av2 set array. The chips were washed and stained with streptavidin phycoerythrin (SAPE; Molecular Probes, Eugene, OR). To amplify staining, streptavidin phycoerythrin solution was added twice with an antistreptavidin biotinylated antibody (Vector Laboratories, Burlingame, CA) staining step in between. The probe array was scanned on a Hewlett-Packard confocal microscope scanner (Hewlett Packard Gene Array Scanner; Hewlett Packard Corporation, Palo Alto, CA) at the excitation wavelength of 488 nm. The amount of light emitted at 570 nm was proportional to the bound target at each location on the probe array. After hybridization and scanning, the microarray images were analyzed using Microarrray Suite 4.0 ® (Affymetrix Inc. Santa Clara, CA) and Gene spring 4.0® (Silicon Genetics, Inc., Redwood City, CA) software. All samples were prepared as described and hybridized onto the Affymetrix Murine Genome U74Av2 Set array, which represents nearly 36,000 full-length murine genes and EST sequences. Each chip contains 16–20 oligonucleotide probe pairs per gene or cDNA clone. A significant fold change (FC) was considered at an average change of ≥2.0. The FC calculations include a series of statistical parameters considering background and noise intensity within each gene chip (Affymetrix GeneChip® Expression Analysis Technical Manual Appendix 5, 1999, Affymetrix, Inc. Santa Clara, CA). The software calculates an average of the two images, defines the probe cells and computes intensity for each cell.

Immunoblot

The treated and non-treated muscle was placed in lysis buffer (8M urea/2% chaps with proteinase inhibitor) on ice. The muscle tissue was then homogenized using a tissue homogeniser (Tekmar Tissumizer model SDT-1810) and placed directly on ice. The homogenized slurry was transferred to a clean tube and centrifuged at 15,000 rpm for 10 min at 4°C (Eppendorf centrifuge 5801 R). The supernatant was aliquoted to sterile microcentrifuge tubes. Protein concentrations were measured using the Bio-Rad Protein Assay with bovine serum albumin as the standard. The aliquoted samples were kept at 80°C until used. Total protein (100 μg) of the sample was electrophoresed on 4%–10% SDS-PAGE gel and then transferred onto nitrocellulose membrane (Bio-Rad). Heat-shocked HeLa cell extract (LYC-HL101F, StressGen) was run as a positive control. The nitrocellulose membrane was blocked with 5% non-fat dry milk in TBST buffer (20 mM Tris-HCl, 150 mM NaCl, pH 7.4) containing 0.1% Tween 20 overnight and then probed with the anti-HSP70 monoclonal antibody (Alkaline phosphated conjugated SPA-810 AP, StressGen). Immunodetection of the protein was achieved through use of an ECF reagent (Amersham/Vistra) according to the manufacturer's protocol and imaged on a phospher imager (Amersham).

Statistical analysis

In order to test the signal intensity changes, the differences of the diffusion coefficient and the T2 time, the statistical analysis was carried out using the U-test, assuming a significance level of <5%. The volume of the devascularized non-contrast enhancing area and the contrast-enhancing area of the muscle tissue treated with continuous wave HIFU or short-pulsed wave HIFU was compared. The statistical analysis was carried out using the U-test, assuming a significance level of <5%. The statistical analysis comparing the relative gene expression levels (fold change, FC) of genes of the continuous wave HIFU and the short-pulsed wave HIFU treated muscle tissue to the untreated contralateral controls was carried out using the U-test, too, assuming a significance level of <5%. In addition, the fold change of the continuous wave HIFU muscle tissue was compared to the short-pulsed wave HIFU-treated muscle tissue.

Table 2 The SNR values of the T1 and T2 images, the diffusion coefficient and the T2 time before and after the application of HIFU

	No HIFU	cw–HIFU		pw–HIFU		U-test cw-pw
	Mean ± SD	Mean ± SD	Difference to no HIFU (%)	Mean ± SD	Difference to no HIFU (%)	(p)
SNR (T2)	6.9±1.2	16.2±2.1	234.2±12.1	15.3±2.1	221.7±13.7	0.21
SNR (T1)	8.9±1.3	7.9±1.3	–11.2±16.5	8.4±0.9	–5.6±10.7	0.12
SNR (T1+CM)	18.4±1.2	20.1±2.4	9.2±9.6	27.4±1.5	48.9±5.5	<0.01
D (mm^{-3}/s)	0.85±0.02	1.37±0.09	161.2±7.1	1.22±0.06	143.5±4.9	0.01
T2 time (ms)	35.5±1.8	117.5±16.6	331.0±14.1	98.3±7.7	276.9±7.8	0.02
Devascularized volume (cm^3)	8.2±2.4		4.5±2.6		<0.01	
Contrast-enhanced volume (cm^3)	5.4±2.5		9.3±3.4		<0.01	

Results

MRI

The MR images showed differences between the muscle tissue treated with continuous wave HIFU and short-pulsed wave HIFU. The T2-weighted images showed a very heterogenous signal intensity in the treated muscle. This heterogeneity was slightly more prominent in the continuous wave mode than in the pulsed wave mode; however, the SNR (T2) values were statistically not significantly different ($p=0.21$). The T2 time was higher in the continuous wave HIFU-treated muscle tissue and statistically significantly different compared to the short-pulsed HIFU wave mode ($p=0.02$). T1-weighted post-contrast images 2 min after i.v. injection of Gd-DTPA in the continuous wave mode showed a diffuse contrast medium enhancement of the tissue with a large non-contrast medium-enhancing area. In the short-pulsed HIFU wave mode the tissue showed also a diffuse contrast medium uptake; however, the non-contrast medium enhancing area was significantly smaller, leading to an overall higher contrast medium uptake ($p<0.01$). A significantly higher diffusion coefficient was found in the muscle tissue treated with continuous wave focused ultrasound as a sign of necrosis. The volume of the devascularized non-contrast-enhancing muscle tissue treated with continuous wave HIFU or short-pulsed wave HIFU differed. The mean volume of the devascularized non-contrast-enhancing muscle tissue treated with continuous wave HIFU was 8.2±2.4 cm^3 versus 4.5±2.6 cm^3 treated with short-pulsed wave HIFU ($p<0.01$). The mean volume of the contrast-enhanced muscle tissue treated with continuous wave HIFU was 5.4±2.5 cm^3 versus 9.3±3.4 cm^3 treated with short pulsed wave HIFU ($p<0.01$) (Table 2) (Fig. 2).

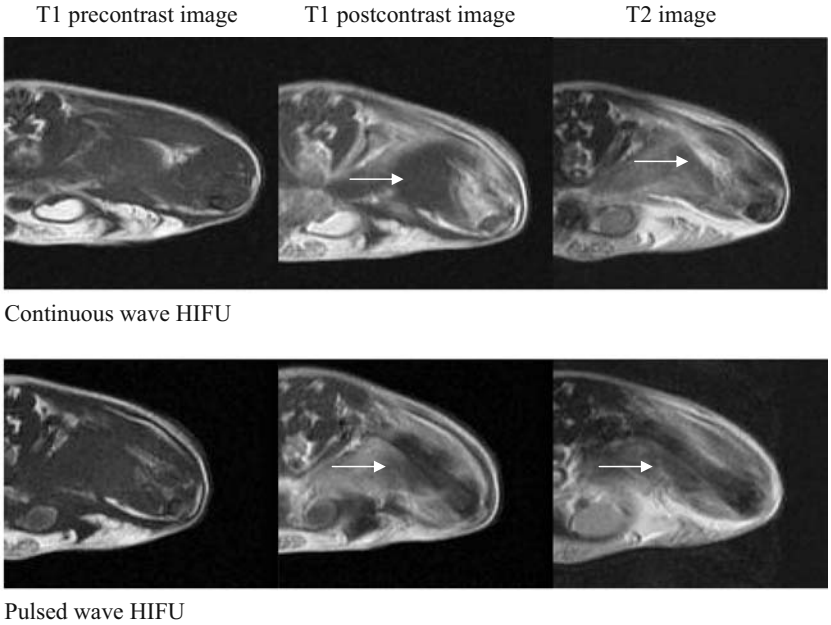

Fig. 2 The arrows of the MR images indicate the changes after application of continuous and short-pulsed wave HIFU. After the application of continuous wave HIFU the post-contrast T1-weighted images showed no contrast uptake in the center, indicating devascularization. In the short-pulsed HIFU wave mode, the contrast medium uptake was almost in the whole treated area. The T2-weighted images showed a very heterogenous signal intensity in the treated muscle

Histology and immunohistochemistry

Tissue not exposed to focused ultrasound was homogenous in histopathology (H&E). No heat shock protein 70 was expressed in muscle tissue prior to HIFU. In the samples treated with focused ultrasound, the continuous wave HIFU mode revealed necrosis in the center of the treated area in H&E stained sections. At the margins the cells appeared to be very compact and dense. Immunohistochemistry revealed high expression of heat shock protein 70. In the short-pulsed wave HIFU mode of focused ultrasound, the H&E staining showed multifocal and coalescing foci of acute coagulation necrosis. Cells comprising these irregular necrotic areas are characterized by condensation and pyknosis of nuclear chromatin and shrinkage and hypereosinophilia of cell cytoplasm. In addition, a higher heat shock protein 70 expression could be detected in these sections (Fig. 3).

Microarray analysis

Gene expression analysis revealed profound changes in expression levels of 26 genes being up-regulated and 12 genes being down-regulated in the continuous wave and 32 genes being up-regulated and 3 genes being down-regulated in the pulsed wave HIFU-treated muscle tissue. The genes after application of pulsed wave HIFU were higher up-regulated than after application of continuous wave HIFU. These genes are related to reaction to ischemia, immune system and inflammation, replication of DNA, transcription and protein synthesis, signal transduction and regulation of gene expression, regulation of cell cycle and cell proliferation, metabolism and surface proteins and receptors. Three genes encoded for heat shock (HSP 70, HSP 40) or related (MHC class III) proteins. The highest degree of up-regulation in both applied modes occurred for HSP 70 (cw FC=49.6±9.8, $p<0.01$; pw FC=75.3±85.0, $p<0.01$), HSP 40 (cw FC=12.3±15.0, $p<0.01$; pw FC=18.1±19.4, $p<0.01$), and its related MHC class III gene (cw FC=31.3±37.4, $p<0.01$; pw FC=83.7±67.4, $p<0.01$). The GRO1 oncogene (cw FC=29.2±12.8, $p<0.01$; pw FC=13.3±14.9, $p<0.01$), FBJ osteosarcoma related oncogene (cw FC=20.6±12.8, $p<0.01$; pw FC=20.1±16.6, $p<0.01$), early growth response 1 (cw FC=18.9±9.7, $p<0.01$; pw FC=13.5±12.8, $p<0.01$), and eukaryotic translation elongation factor 1 alpha 2 (cw FC=8.1±1.4, $p\leq0.01$; pw FC=12.0±1.2, $p\leq0.01$) were also highly up-regulated genes in both modes. A few genes were more highly up-regulated after application of continuous wave HIFU. These genes were the cytotoxic T lymphocyte-associated protein 2 alpha (cw FC=11.2±18.1, $p\leq0.01$; pw FC=2.7±0.4, $p=0.02$), the fibroblast inducible secreted protein (cw FC=5.2±2.1, $p=0.02$; pw FC=1.5±0.3, $p=0.45$), and the ATPase, Ca++ transporting, cardiac muscle fast twitch 1 (cw FC=5.0±9.8, $p=0.01$; pw FC=2.0±0.5, $p=0.2$).

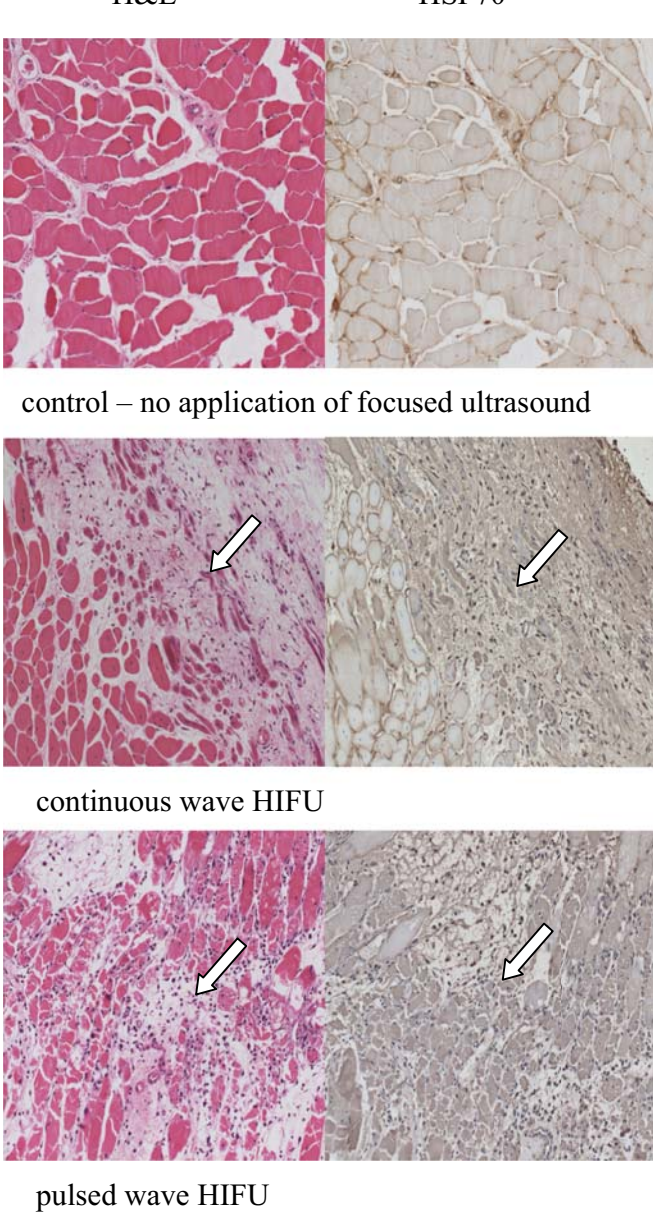

Fig. 3 Tissue not exposed to focused ultrasound was homogenous in histopathology (H&E). No heat shock protein 70 was detected. In the continuous wave HIFU mode the H&E staining revealed necrosis in the center of the treated area. Immunohistochemistry was positive for HSP70. In the short-pulsed wave HIFU mode H&E staining showed multifocal and coalescing foci of acute coagulation necrosis. Immunohistochemistry was positive for HSP70, too

The most down-regulated genes related to the immune system, inflammation and metabolic processes were seen after application of the continuous mode of HIFU. These genes were for instance the histocompatibility 2, class II antigen A. alpha (cw FC=−32.5±49.5, $p\leq0.01$; pw FC=1.2±3.0, $p=0.13$), the calpactin I light chain (cw FC=−12.8±21.1, $p\leq0.01$; pw FC=−0.7±3.8, $p=0.65$), or the

Mus musculus proteasome alpha7/C8 subunit mRNA (cw FC=−8.1±5.0, p≤0.01; pw FC=0.3±1.4, p=0.65), and the glyceraldehyde-3-phosphate dehydrogenase (cw FC=−7.0±12.3, p=<0.01; pw FC=1.5±0.3, p=0.34) (Table 3).

Immunoblot

In accordance with the gene expression changes the Immunoblot analysis showed similarities in the protein products between the tissues exposed to the continuous HIFU mode and to the short-pulsed HIFU mode. In the tissue lysate of the muscle cells HSP70 protein was detectable in the samples when continuous and short-pulsed HIFU was applied. The detection of the HSP70 protein expression is, however, not immediately possible after focused ultrasound exposure [Fig. 4, lane 4 (cw) and lane 5 (pw)]. Four hours later, the Immunoblot analysis revealed the presence of the HSP 70 protein [Fig. 4, lane 6 (cw-4 h) and lane 7 (pw-4 h)]. Confirming that the gene expression analysis revealed high up-regulation of the HSP 70 gene led to an increased synthesis of the HSP 70 protein.

Discussion

High intensity focused ultrasound (HIFU) treatment of mouse muscle tissue provides a model system to study gene expression patterns at different modes of energy deposition. HIFU treatment causes physical changes in tissues through energy deposition. A major advantage of this technique is that it is noninvasive and does not require the insertion of probes. The non-invasive nature of this technique keeps tissue intact for further evaluation after treatment. The mode of focused ultrasound application has a major impact on the tissue. McDannold [20] showed that the time between the sonication has an important influence. With a short intersonication delay the extent of tissue coagulation increased; with a longer delay the destroyed tissue was uniform, and the temperature build-up was substantially lower. To further correlate biological changes in the tissue in response to HIFU treatment mode to imaging changes, we have chosen two different modes: the continuous HIFU mode with a frequency of 1 MHz applied for 20 s and the short-pulsed HIFU mode with a frequency of 0.5 Hz applied for 16.5 min. The goal was to see if the different modes have a different impact on the tissue as evaluated by MRI, histopathology and functional gene analysis. In our study we found that MRI changes were different using the short-pulsed HIFU mode compared to the continuous wave mode. In the T1-weighted images, the contrast agent uptake was lower, due to a larger devascularized area in the continuous wave mode than in the short-pulsed mode. It could be shown that a partial or complete lack of contrast material uptake on post-contrast T1-weighted images implies devascularization and tissue necrosis. The T2 signal intensity, T2 time and the diffusion coefficient was also increased applying the continuous HIFU mode. These MRI parameters are additional indicators that the tissue was more damaged in the continuous wave mode. Other studies showed a higher T2 signal intensity [21] and a higher diffusion coefficient [22] in tissue, which is an indication of more pronounced necrosis in the tissue. Histological analysis showed that, applying the continuous HIFU mode, large areas of muscle tissue were destroyed. In the necrotic tissue no viable muscle fibers were seen. Lymphocytes and macrophages were seen in the area. In the short-pulsed HIFU mode, muscle necrosis was seen beside damaged, but viable muscle fibers. This is an indication that the short-pulsed HIFU mode did not damage the tissue so severely as the continuous wave mode. It has to be considered that the damaging effect of the continuous wave mode is due to thermal effects [23] leading to a larger devascularised area.

We presume that the damaging effect of the pulsed wave mode is not due to thermal effects because the pulse was only 50 ms every 2 s and cooling effects took place in the water bath between the sonication pulses. In the pulsed mode cavitation effects and mechanical effects were the most damaging effects [23]; however this damaging effect is not so high as the damaging effect of the continuous wave mode of HIFU so that viable tissue will be spared. Tissue necrosis is inhomogeneous in the present study, as seen in MR imaging and in histology. This phenomenon is due to the heterogeneity of heat deposition and the heterogeneity of deposition of the short pulses in the muscle tissue and was also seen in histopathology after treatment of a localized adenocarcinoma of the prostate [24] and in ablation of liver tissue [25]. Dittmar [26] showed in a DNA delivery experiment in the SCCVII tumor cell line with similar HIFU parameters an increase of GFP uptake in the tumor cell without any destructive effect to the tumor tissue, and Yuh [27] could show in a drug delivery experiment in a tumor model with similar parameters that pulsed high-intensity focused ultrasound does increase drug delivery to tumor tissue. This can be explained by the fact that tumor tissue is much more rigid than muscle tissue, and it takes more energy in order to damage the tissue.

Oligonucleotide microarray analysis allows simultaneous examination of a large number of genes. This provides an unbiased evaluation of the expressed genes in a particular system. Thus, it serves as an efficient way to discover potential targets for imaging diagnosis and therapeutics. Gene expression analysis revealed profound gene expression changes in both modes of HIFU of the treated muscle tissue. The same genes were up-regulated after application of both HIFU modes, indicating that the gene up-regulation is independent of the damaging effect of the HIFU therapy.

However, genes were down-regulated only after application of the continuous wave of HIFU, indicating that the tissue was so severely damaged that different metabolic processes were significantly suppressed. In our study, despite the fact that we saw a similar gene expression

Table 3 Gene expression profile of muscle treated with focused ultrasound. The statistical analysis of the gene expression profiles for the muscle tissue treated with HIFU showed that statistically significant differences in gene expression were seen between muscle tissue treated with continuous wave and those treated with short-pulsed wave HIFU

Gene name	Acc. #	cw		pw		
		FC±SD	t-test cw vs. normal	FC ± SD	t-test pw vs. normal	t-test cw vs. pw
1. Reaction to ischemia						
Heat shock protein 70 kDa 3	M12571	49.6±9.8	<0.01	75.3±85.0	<0.01	<0.01
Mus musculus hsp40 mRNA for heat shock protein 40	AB028272	12.3±15.0	<0.01	18.1±19.4	<0.01	0.02
2. Immune system and inflammation						
Mouse mRNA with a set 1 repetitive element for a class I major histocompatibility complex (MHC) antigen	X00246	–14.3±24.3	<0.01	0.4±1.9	0.44	<0.01
Histocompatibility 2. class II antigen A. alpha	X52643	–32.5±49.5	<0.01	1.2±3.0	0.13	<0.01
Histocompatibility 2. T region locus 23	Y00629	–5.9±5.1	0.01	2.4±0.1	0.04	<0.01
Mus musculus MHC class III region RD gene	AF109906	31.3±37.4	<0.01	83.7±67.4	<0.01	<0.01
Interleukin 6		14.2±7.3	0.005	20.3±14.9	0.000	0.005
Mus musculus intracellular calcium-binding protein (MRP8) mRNA	M83218	4.9±3.1	0.02	11.3±3.8	<0.01	<0.01
Chemokine (C-X-C motif) ligand 1 (melanoma growth-stimulating activity. alpha) (GRO1 oncogene)	J04596	29.2±12.8	<0.01	13.3±14.9	<0.01	<0.01
A disintegrin-like and metalloprotease (reprolysin type) with thrombospondin type 1 motif. 1	M62470	5.8±2.2	0.03	5.5±0.1	0.04	0.24
Mast cell protease 2	J05177	2.4±0.5	0.03	1.4±0.2	0.46	0.23
Suppressor of cytokine signaling-3 (SOCS-3)		7.7±3.4	0.003	25.7±6.9	0.000	0.003
CD14 antigen	X13333	0.7±4.6	0.053	4.5±1.7	<0.01	0.03
Annexin A1/ lipocortin 1	M69260	2.1±0.5	0.04	0.6±2.3	0.23	0.34
Cytotoxic T lymphocyte-associated protein 2 alpha	X15591	11.2±18.1	<0.01	2.7±0.4	0.02	<0.01
T-cell specific GTPase	L38444	2.3±1.3	0.03	2.5±2.3	0.03	0.34
Calpactin I light chain	M16465	–12.8±21.1	<0.01	–0.7±3.8	0.65	<0.01
Fibrinogen-like protein 2	M16238	2.1±2.3	0.04	5.0±3.2	0.01	0.02
Interferon inducible GTPase 1	AJ007971	0.1±1.1	0.41	3.1±1.1	0.02	0.34
3. Replication of DNA, transcription, protein synthesis						
Mus musculus ribosomal protein L41 mRNA	U93862	3.1±1.2	0.02	1.3±0.1	0.35	0.32
CCAAT/enhancer binding protein (C/EBP). Delta	X61800	2.5±0.1	0.03	-3.0±3.0	0.03	0.02
Eukaryotic translation elongation factor 1 alpha 2	L26479	8.1±1.4	<0.01	12.0±1.2	<0.01	0.01
Mus musculus transcription factor junB (junB) gene	U20735	1.2±0.7	0.65	5.8±1.1	<0.01	0.02
Mus musculus putative transcriptional regulator	AF013282	1.3±0.9	0.37	5.2±4.2	<0.01	0.01
Mus musculus transcription factor LRG-21 mRNA	U19118	7.6±3.5	<0.01	8.8±6.7	<0.01	0.14
4. Signal transduction and regulation of gene expression						
Mus musculus retinoic acid-inducible E3 protein mRNA	U29539	–4.2±1.2	0.01	6.1±2.8	<0.01	<0.01
Mus musculus Ras-like GTP-binding protein Rad mRNA	AF084466	4.1±0.2	0.01	8.1±9.9	<0.01	0.03
5. Regulation of cell cycle and cell proliferation						
Insulin-like growth factor 10	M32490	3.5±2.1	0.01	2.0±1.1	0.06	0.31
Mouse mRNA for profilin	X14425	0.5±1.4	0.34	–8.2±6.2	<0.01	<0.01
Actin alpha 1. skeletal muscle	M12347	1.0±2.1	0.15	2.1±0.1	0.04	0.21
Epithelial membrane protein 3	U87948	–3.4±2.2	0.04	–0.4±1.2	0.65	0.02

Table 3 (Continued)

Gene name	Acc. #	cw		pw		
		FC±SD	t-test cw vs. normal	FC ± SD	t-test pw vs. normal	t-test cw vs. pw
Fibroblast inducible secreted protein	M70642	5.2±2.1	0.02	1.5±0.3	0.45	0.01
ATPase. Ca++transporting. cardiac muscle. fast twitch 1	X67140	5.0±9.8	0.01	2.0±0.5	0.21	0.04
Metallothionein 2	K02236	2.1±3.8	0.04	5.4±1.7	0.01	0.02
Metallothionein 1	V00835	0.9±5.3	0.65	8.0±7.2	<0.01	0.01
FBJ osteosarcoma-related oncogene	V00727	20.6±12.8	<0.01	20.1±16.6	<0.01	0.31
Early growth response 1	M28845	18.9±9.7	<0.01	13.5±12.8	<0.01	0.23
Similar to myosin light polypeptide 6 (myosin light chain alkali 3) (myosin light chain 3) (MLC-3) (LC17)	X12972	–5.8±9.5	<0.01	-0.7±1.1	0.21	0.01
Mus musculus pigment epithelium-derived factor (PEDF) mRNA	AF036164	–1.2±2.1	0.32	5.0±8.8	<0.01	0.01
6. Netabolism						
S-adenosylmethionine decarboxylase 3	Z23077	–2.4±1.2	0.04	–0.8±2.2	0.23	0.21
Mus musculus adipocyte specific protein adipoQ (adipoQ) mRNA	U49915	–0.6±4.2	0.53	2.9±6.4	0.03	0.07
Hemoglobin beta. adult chain 1	V00722	4.1±3.3	0.02	2.5±0.9	0.04	0.01
Aminolevulinic acid synthase 2. erythroid	M15268	15.9±9.2	<0.01	4.9±4.6	0.01	0.01
Apolipoprotein E	D00466	0.4±2.5	0.62	–4.9±1.2	0.02	0.01
Pyruvate dehydrogenase E1 alpha 1	M76727	2.5±1.3	0.04	1.1±0.1	0.34	0.12
Mus musculus proteasome alpha7/C8 subunit mRNA	AF055983	–8.1±5.0	<0.01	0.3±1.4	0.65	0.01
Glyceraldehyde-3-phosphate dehydrogenase	M32599	–7.0±12.3	<0.01	1.5±0.3	0.34	0.01
Mouse gene for ferritin H subunit	X52561	–5.4±4.0	<0.01	0.4±1.3	0.34	0.01
Annexin XI	U65986	–5.2±4.7	<0.01	0.3±1.5	0.45	0.01
TYRO protein tyrosine kinase-binding protein	AF024637	–0.5±0.1	0.56	5.0±2.8	<0.01	0.01
Hyaluronan synthase1	D82964	1.3±2.9	0.64	5.1±2.7	<0.01	0.03
Mus musculus putative RNA helicase RCK mRNA	AF038995	0.9±2.9	0.45	5.7±5.8	<0.01	0.01
7. Surface proteins and receptors						
Mus musculus Xin mRNA	AF051945	2.5±0.4	0.08	1.1±1.9	0.35	0.21
8. Unknown function						
Mouse pseudogene for alphaglobin without intervening sequences	V00716	5.3±3.2	0.03	3.3±1.6	0.04	0.24

pattern applying the continuous HIFU mode and the short-pulsed HIFU mode in muscle tissue, gene expression was overall higher applying the short-pulsed HIFU mode. This might be explained in that the overall damaging effect, leading to an incomplete ablation of the muscle tissue, was not so severe in the short-pulsed HIFU mode, so that the tissue was able to react with a higher gene up-regulation than in the more severely damaged tissue after application of continuous wave mode of HIFU leading to an immediate cell denaturation of the muscle tissue.

Up-regulated genes are related to stress and ischemia, inflammation, immunity and signal transduction and growth and gene regulation. The heat shock proteins (HSPs) are a family of molecular chaperones induced by environmental stresses such as oxidative injury and contribute to protection from and adaptation to cellular stress [28]. It has a cytoprotective role in a variety of diseases mediated by ischemia, inflammation, and infection [29]. The cardioprotective role of heat shock proteins is a well-established fact [30]. Experiments with heat shock protein induction with hyperthermia, their overexpression in transgenic mice and direct transfer into the myocardium has shown that these proteins could render the heart resistant to an ischemic insult [31]. This high up-regulation of the HSP70 gene expression led to a direct increase in the production of the HSP70 protein itself. This could be confirmed by immunohistochemistry and immunoblot analysis in the muscle tissue treated with the continuous as well as treated with the short-

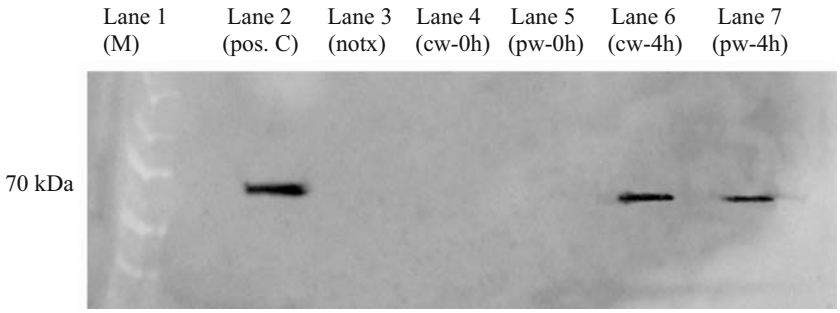

Fig. 4 Immunoblot analysis of the HSP70 expression in muscle tissue: lane 1-marker proteins (M), Biorad; lane 2-positive heat shock cell lysate (pos C), product # LYC-HL101, StressGene; lane 3-muscle tissue cell lysate not exposed to focused ultrasound treatment (notx); lane 4-continuous wave-treated muscle tissue cells harvested directly after the application (cw); lane 5-short-pulsed wave-treated muscle tissue cells harvested directly after the application (pw); lane 6-continuous wave-treated muscle tissue cells harvested after 4 h (cw-4 h); lane 7-pulsed wave-treated muscle tissue cells harvested after 4 h (pw-4 h)

pulsed HIFU mode. However, the protein cannot be detected directly after the application of focused ultrasound. Four hours lapsed between the time of HIFU application and the detection of a significant amount of protein product as evaluated by Immunoblot analysis. It is known that HSP 40 functions together with HSP 70 as a molecular chaperone; this is necessary for assembly and disassembly of the protein complexes and protein folding [32]. The major histocompatibility complex (MHC), interleukin 6, GRO1 oncogene, and the suppressor of cytokine signaling (SOCS-3) gene involved in inflammation, immunity and signal transduction showed a significant up-regulation. MHC [33] plays a central role initiating both the humoral and cell-mediated immunity. The MHC class III region contains many genes with varying functions. It has been proposed that the MHC region is an immunologic gene cluster, as many of the gene products are involved in the generation of the immune response [34]. Immediately after tissue injury genes are up-regulated, which promotes tissue restoration. The higher up-regulation of MHC class III applying the short-pulsed HIFU indicates that more tissue restoration processes are under way. Cytokines are key players in the regulation of the immune responses. Interleukin 6 (IL-6) is obviously one of the earliest and most important mediators of short-term phase response. These so-called IL-6-type cytokines play an important role in the regulation of complex cellular processes such as gene activation, proliferation, and differentiation [35]. A further important gene is the GRO1 oncogene gene. It was named because it was found at first in melanoma tumors. It induces the production of melanoma growth stimulatory activity (MGSA) [36]. MGSA belongs to a superfamily of proteins that includes interleukin-8 (IL8) and platelet factor-4 (PF4). These proteins are in general involved in inflammatory processes [37]. It also promotes tumor growth, metastasis, and angiogenesis [38]. GRO 1 expression can be induced by interleukin-1 and early growth response [39]. In our study, interleukin-1 was not highly up-regulated; however, early growth response 1 showed a 18.9±9.7- and 13.5±12.8-fold change increase compared to non-treated muscle tissue.

Suppressors of cytokine signaling (SOCS) are a newly identified family of intracellular proteins controlling the magnitude and/or duration of signals propagated by diverse cytokine receptors through suppressing their signal transduction process [40]. Since their expression is induced by the same cytokine-/receptor-mediated signal transduction pathway that subsequently inhibits the SOCS proteins, this represents an intracellular negative feedback loop in the cytokine signaling process [41].

The FBJ osteosarcoma oncogene, the early growth response, and the δ-aminolevulinic acid synthase (ALA synthase) are important for growth gene regulation and metabolism. They respond immediately to tissue injury. FBJ osteosarcoma oncogene is a nuclear phosphorprotein and has a critical function in regulating the development of cells destined to form and maintain the skeleton. It is thought to have an important role in signal transduction, cell proliferation, and differentiation. FBJ osteosarcoma oncogene expression increases upon a variety of stimuli, including growth factors, cytokines, neurotransmitters, polypeptide hormones, stress and cell injury [42]. The lack of contrast uptake in the continuous HIFU mode-treated muscle tissue is a sign of devascularization leading to ischemia of the tissue. The tissue responds with the up-regulation of genes to overcome the ischemia. In our study two genes were up-regulated related to heme synthesis, the δ-aminolevulinic acid synthase and the hemoglobin beta adult chain 1.

The zinc-finger transcription factor early growth response 1 (EGR-1) is an important early reaction factor in the cascade of hypoxia associated tissue changes [43]. In our study the zinc finger protein was also up-regulated in the continuous wave slightly more than in the short-pulsed HIFU mode. Egr-1 expression is associated with endothelial injury [44] and coupled with endothelial cell proliferation and can be activated by growth factors like basic fibroblast growth factor (β-FGF) [45]. In addition, Egr-1 up-regulates the expression of platelet-derived growth factor (PDGF), the VEGF-receptor Flt-1 [46], and it triggers the expression of VEGF itself [47]. It has also been

implicated to have a role in the expression of tissue factor, resulting in fibrin deposition (hypoxia). Early growth response 1 is additionally involved in controlling cell growth. It is rapidly induced after stimulation of quiescent cells with a variety of stimuli [48].

These targets related to ischemia, inflammation, immunity, signal transduction and restoration can be candidates for molecular imaging and therapeutic targets. There are a few papers published utilizing molecular targets for therapeutic applications. Pachori [49] developed successfully a pre-emptive strategy for tissue protection using an adeno-associated vector system containing erythropoietin hypoxia response elements for ischemia-regulated expression of the therapeutic gene human heme-oxygenase-1 (hHO-1). They demonstrate that a single administration of this vector several weeks in advance of ischemia/reperfusion injury to multiple tissues such as heart, liver, and skeletal muscle yields rapid and timely induction of hHO-1 during ischemia that resulted in dramatic reduction in tissue damage. They selected the HO-1 as a therapeutic target from among many other potential therapeutic genes, such as superoxide dismutase [50], nitric oxide synthase [51], and vascular endothelial growth factor [52] on the basis of its documented cytoprotective effects [53] for the purpose of demonstrating the feasibility and therapeutic potential of this strategy with a validated cardioprotective gene. However, they emphasize that this strategy can be extended to the expression of any gene or combination of gene(s) with therapeutic value for protection from ischemia-induced injury. In our study we saw also an up-regulation of the suppressor of cytokine signaling-3. Karlsen [41] mentioned in his study that because of the function of SOCS-3 as regulator of cytokine action having an influence on the cellular fate after cytokine exposure (e.g., influence metabolism, proliferation and apoptosis), it might be an attractive candidate for an intercellular negative feedback mechanism.

A further therapeutic target might be the zinc-finger transcription factor early growth response (Egr)-1. It functions as a master switch activated by ischemia to trigger expression of pivotal regulators of inflammation, coagulation and vascular hyper-permeability. Yan [43] showed that the deletion of the gene encoding Egr-1 strikingly diminished expression of these mediators of vascular injury in a murine model of lung ischemia/reperfusion and enhanced animal survival and organ function. He proposed that short-term antagonism of Egr-1 may provide an unexpected therapeutic target to diminish maladaptive host responses incited by acute ischemia.

In this context microarray analysis gives the opportunity to look for a whole variety of potential targets. MRI information gives estimation for the degree of tissue change with the possibility to get a better understanding of ongoing biological processes. The combination of histological and microarray analysis complements the observed changes on MRI and adds biological context to these changes.

References

1. Bednarski MD, Lee JW, Callstrom MR et al (1997) In vivo target-specific delivery of macromolecular agents with MR-guided focused ultrasound. Radiology 204(1):263–268
2. Kendell KR, Wu T, Felmlee JP, Lewis BD, Ehman RL (1998) MR-guided focused-ultrasound ablation system: determination of precision and accuracy in preparation for clinical trials. Radiology 209(3):856–861
3. Lejbkowicz F, Salzberg S (1997) Distinct sensitivity of normal and malignant cells to ultrasound in vitro. Environ Health Perspect 105(Suppl 6):1575–1578
4. Hrazdira I, Skorikova J, Dolnikova M (1999) Ultrasonically induced alterations of cultured tumor cells. Eur J Ultrasound 8:43–49
5. Alter A, Rozenszajn LA, Miller HI, Rosenschein U (1998) Ultrasound inhibits the adhesion and migration of smooth muscle cells in vitro. Ultrasound Med Biol 24:711–721
6. Doan N, Reher P, Meghji S, Harris M (1999) In vitro effects of therapeutic ultrasound on cell proliferation, protein synthesis and cytokine production by human fibroblasts, osteroblasts and monocytes. J Oral Maxillofac Surg 57:409–419
7. Vaupel P (1990) Pathophysiological effects of hyperthermia in cancer therapy gauthrie M (Hrsg.): methods of external hyperthermic heating. Springer Berlin, Heidelberg New York, pp 73–126
8. Chen WS, Lafon C, Matula TJ, Vaezy S, Crum LA (2003) Mechanisms of lesion formation in high intensity focused ultrasound therapy. Acoust Res Letter Online 4:41–46
9. Barnett SB, ter Haar GR, Ziskin MC, Nyborg WL, Maeda K, Bang J (1994) Current Status of Research on Biophysical Effects of Ultrasound. Ultrasound Med Biol 20:205–218
10. McNeil PL, Terasaki M (2001) Coping with the inevitable: how cells repair a torn surface membrane. Nature Cell Biol 3:E124–E129
11. Schreiber S. Mechanisms of Cell Death. http://www.ucihs.uci.edu/anatomy
12. Karu T (1998) The science of low-power laser therapy. Gordon & Breach, New York
13. Yu W, McGowan M, Ippolito K et al (1997) Photomodulation of oxidative metabolism and electron chain enzymes in rat liver mitochondria. Photochem Photobiol 66:866–871
14. Benjamin IJ, McMillan DR (1998) Stress (heat shock) proteins: molecular chaperones in cardiovascular biology and disease. Circ Res 83:117–132
15. Bibikova A, Oron U (1993) Promotion of muscle regeneration in the toad (Bufo viridis) gastrocnemius muscle by low energy laser irradiation. Anat Rec 235:375–380
16. Marber MS, Mestril R, Chi S-H et al (1995) Overexpression of the rat inducible 70-kD heat stress protein in a transgeneic mouse increases the resistance of the heart to ischemic injury. J Clin Invest 95:1446–1456

17. Wallen ES, Buettner GR, Moseley PL (1997) Oxidants differentially regulate the heat shock response. Int J Hyperthermia 13:517–524
18. Clement GT (2004) Perspectives in clinical uses of high-intensity focused ultrasound. Ultrasonics 42(10):1087–1093
19. Boetes C, Mus RD, Holland R, Barentsz JO, Strijk SP, Wobbes T, Hendriks JH, Ruys SH (1995) Breast tumors: comparative accuracy of MR imaging relative to mammography and US for demonstrating extent. Radiology 197:743–747
20. McDannold N, Jolesz F, Hynynen K (1996) Determination of the optimal delay between sonications during focused ultrasound surgery in rabbits by using mr imaging to monitor thermal buildup in Vivo. Radiology 211:419–426
21. Guccione S, Yang YS, Shi G, Lee DY, Li KC, Bednarski MD (2003) Functional genomics guided with MR imaging: mouse tumor model study. Radiology 228(2):560–568
22. Ross RD, Moffat BA, Lawrence TS et al (2003) Evaluation of cancer therapy using diffusion magnetic resonance imaging. Molecular Cancer Therapeutics 2:81–587
23. ter Haar G (2007) Therapeutic applications of ultrasound. Prog. Biophys Mol Biol 93(1–3):11–129. Jan-Apr
24. Van Leenders GJLH, Beerlage HP, Ruijter ETH, de la Rosette JJMCH, van de Kaa CA (2000) Histopathological changes associated with high intensity focused ultrasound (HIFU) treatment for localised adenocarcinoma of the prostate. J Clin Pathol 53:391–394
25. Yu T, Fan X, Xiong S, Hu K, Wang Z (2006) Microbubbles assist goat liver ablation by high intensity focused ultrasound. Eur Radiol 16:1557–1563
26. Dittmar KM, Xie J, Hunter F, Trimble C, Bur M, Frenkel V, Li KC (2005) Pulsed High-Intensity Focused Ultrasound Enhances Systemic Administration of Naked DNA in Squamous Cell Carcinoma Model: Initial Experience. Radiology 235:541–546
27. Yuh EL, Shulman SG, Mehta SA, Xie J, Chen L, Frenkel V, Bednarski MD, Li KC (2005) Delivery of systemic chemotherapeutic agent to tumors by using focused ultrasound: study in a murine model. Radiology 234:431–437
28. de Vera ME, Wong JM, Zhou JY et al (1996) Transcription is blocked by the heat shock response in human liver cells. Surgery 120:144–149
29. Frydman J, Nimmesgern E, Ohtsuka K et al (1994) Folding of nascent polypeptide chains in a high molecular mass assembly with molecular chaperones. Nature 370(6485):111–117
30. Currie RW, Karmazyn M, Kloc M et al (1988) Heat-shock response is associated with enhanced postischemic ventricular recovery. Circ Res 63:543–549
31. Okubo S, Wildner O, Shah MR et al (2001) Gene transfer of heat-shock protein 70 reduces infarct size in vivo after ischemia/ reperfusion in rabbit heart. Circulation 103:877–881
32. Campbell RD, Trowsdale J (1993) Map of the human MHC. Immunol Today 14 (7):349–352 Jul
33. Samarel AM (2002) IGF-1 Overexpression rescues the failing heart. Circ Res 90(6):631–633
34. Fortier LA, Mohammed HO, Lust G, Nixon AJ (2002) Insulin-like growth factor-I enhances cell-based repair of articular cartilage. J Bone Joint Surg Br 84(2):276–288
35. Heinrich P, Behrmann I, Mueller-Newen G et al (1998) Interleukin-6-type cytokine signalling through the gp130/Jak/STAT pathway. Review Biochem J 334:297–314
36. Horuk R, Yansura DG, Reilly D et al (1993) Purification, receptor binding analysis, and biological characterization of human melanoma growth stimulating activity (MGSA): evidence for a novel MGSA receptor. J Biol Chem 268:541–546
37. Richmond A, Balentien E, Thomas HG et al (1988) Molecular characterization and chromosomal mapping of melanoma growth stimulatory activity, a growth factor structurally related to beta-thromboglobulin. EMBO J 7:2025–2033
38. Smith CW, Chen Z, Dong G et al (1998) The host environment promotes the development of primary and metastatic squamous cell carcinoma that constitutively express proinflammatory cytokines, IL-1 IL-6, GM-CSF and KC. Clin Exp Metastasis 16:655–664
39. Loukinova E, Dong G, Chen Z, Sunwoo J, Van Waes C (2000) Constitutive activation of a C-X-C chemokine KC promotes metastatic potential in murine squamous cell carcinoma. Oncogene 19:3477–3486
40. Dalpke AH, Opper S, Zimmermann S et al (2001) Suppressors of cytokine signaling (socs)-1 and socs-3 are induced by cpg-dna and modulate cytokine responses in APCs. J Immunol 166(12):7082–7089
41. Karlsen A, Rønn SG, Lindberg K (2001) Suppressor of cytokine signaling 3 (SOCS-3) protects β-cells against interleukin-1-β and interferon-γ-mediated toxicity. PNAS 98 (21):12191–12196
42. Acquaviva C, Bossis G, Ferrara P et al (2002) Evasion from proteasomal degradation by mutated Fos proteins expressed from FBJ-MSV and FBR-MSV osteosarcomatogenic retroviruses. Biochem Pharmacol 64(5–6):957–961
43. Yan SF, Lu J, Zou YS et al (1999) Hypoxia-associated induction of early growth response-1 gene expression. Biol Chem 274(21):15030–15040
44. Khachigian LM, Anderson KR, Halnon NJ, Gimbrone MA Jr et al (1997) Egr-1 is activated in endothelial cells exposed to fluid shear stress and interacts with a novel shear-stress-response element in the PDGF A-chain promoter. Arterioscler Thromb Vasc Biol 17:2280–2286
45. Ko Y, Totzke G, Schiermeyer B et al (1995) Reverse transcriptase-polymerase chain reaction (RT-PCR): a sensitive method to examine basic fibroblast growth factor-induced expression of the early growth response gene-1 (egr-1) in human umbilical arterial endothelial cells. Mol Cell Probes 9:215–222
46. Vidal F, Aragones J, Alfranca A et al (2000) Up-regulation of vascular endothelial growth factor receptor Flt-1 after endothelial denudation: role of transcription factor Egr-1. Blood 95:3387–3395
47. Yan SF, Fujita T, Lu J et al (2000) Egr-1, a master switch coordinating upregulation of divergent gene families underlying ischemic stress. Nat Med 6(12):1355–1361
48. Milbrandt J (1987) A nerve growth factor-induced gene encodes a possible transcriptional regulatory factor. Science 238:797–799
49. Pachori A, Melo L, Hart M et al (2004) Hypoxia-regulated therapeutic gene as a preemptive treatment strategy against ischemia reperfusion tissue injury. PNAS 101(33):12282–12287
50. Woo YJ, Zhang JC, Vijayasarathy C et al (1998) Recombinant adenovirus-mediated cardiac gene transfer of superoxide dismutase and catalase attenuates postischemic contractile dysfunction. Circulation 98:255–260
51. Jones SP, Greer JJ, Kakkar AK et al (2004) Endothelial nitric oxide synthase overexpression attenuates myocardial reperfusion injury. Am J Physiol 286:H276–H282
52. Su H, Arakawa-Hoyt J, Kan YW (2002) Adeno-associated viral vector-mediated hypoxia response element-regulated gene expression in mouse ischemic heart model. Proc Natl Acad Sci 99:9480–9485
53. Nie RG, McCarter SD, Harris KA et al (2002) The role of endogenous heme oxygenase in the initiation of liver injury following limb ischemia/reperfusion. J Hepatol 36:624–630